Published in final edited form as:
Anal Chem. 2013 November 5; 85(21): . doi:10.1021/ac401537k.

Ultrasensitive SERS Flow Detector Using Hydrodynamic Focusing

Pierre Negri, **Kevin T. Jacobs**, **Oluwatosin O. Dada**, and **Zachary D. Schultz***
Department of Chemistry and Biochemistry, University of Notre Dame, Notre Dame, IN 46556

Abstract

Label-free, chemical specific detection in flow is important for high throughput characterization of analytes in applications such as flow injection analysis, electrophoresis, and chromatography. We have developed a surface-enhanced Raman scattering (SERS) flow detector capable of ultrasensitive optical detection on the millisecond time scale. The device employs hydrodynamic focusing to improve SERS detection in a flow channel where a sheath flow confines analyte molecules eluted from a fused silica capillary over a planar SERS-active substrate. Increased analyte interactions with the SERS substrate significantly improve detection sensitivity. The performance of this flow detector was investigated using a combination of finite element simulations, fluorescence imaging, and Raman experiments. Computational fluid dynamics based on finite element analysis was used to optimize the flow conditions. The modeling indicates that a number of factors, such as the capillary dimensions and the ratio of the sheath flow to analyte flow rates, are critical for obtaining optimal results. Sample confinement resulting from the flow dynamics was confirmed using wide-field fluorescence imaging of rhodamine 6G (R6G). Raman experiments at different sheath flow rates showed increased sensitivity compared with the modeling predictions, suggesting increased adsorption. Using a 50-millisecond acquisitions, a sheath flow rate of 180 μL/min, and a sample flow rate of 5 μL/min, a linear dynamic range from nanomolar to micromolar concentrations of R6G with a LOD of 1 nM is observed. At low analyte concentrations, rapid analyte desorption is observed, enabling repeated and high-throughput SERS detection. The flow detector offers substantial advantages over conventional SERS-based assays such as minimal sample volumes and high detection efficiency.

INTRODUCTION

Increased understanding of surface-enhanced Raman scattering (SERS) has expanded the utility of Raman spectroscopy for a variety of applications requiring a high degree of chemical specificity.[1-3] In recent years, SERS has shown tremendous potential as a powerful and ultrasensitive detection technique at the trace and even the single molecule level.[4-8]

One of the benefits of SERS detection is the ability to probe the structural properties of compounds in various physical environments. More particularly, the chemical specificity and insensitivity to water render SERS an ideal candidate for highly sensitive detection of analytes in aqueous environment. These attributes suggest SERS would be an ideal detector for flow injection, electrophoresis, and chromatography applications.

High sensitivity SERS detection in flow has remained challenging. SERS originates from molecules located in close proximity to metallic nanostructures that are capable of

*Author to whom correspondence should be sent tel: +1-574-631-1853 schultz.41@nd.edu.

Supporting Information Available: This material is available free of charge via the Internet at http://pubs.acs.org.

generating a localized surface plasmon resonance (LSPR). As a result, one of the inherent requirements for SERS signal generation is that molecules must be located near the enhancing surface. This distance dependence intrinsic to SERS varies based on the type of nanostructures used for the SERS substrate. For individual nanoparticles the enhancement extends a few nanometers whereas an exponential decay of the evanescent field with a length scale of ~10 nm is observed on extended surfaces.[9-11] Traditionally, depositing a solution onto a metallic nanostructure and allowing it to evaporate adsorbs molecules to the surface. In solution, however, the ability of molecules to diffuse away from the nanostructures results in limited sensitivity. It follows that the number of molecules present in the enhanced region in dilute solution is often below the limit of detection. These effects typically require micromolar or greater solution concentrations.[12]

Nanostructure-analyte interactions in the SERS detection volume are key to improving signal sensitivity. A common approach used to promote this interaction involves mixing of the sample analyte and the colloids, either directly in a microfluidic channel or off-line prior to being introduced in the fluidic system.[13-18] These techniques can achieve high sensitivity and are known to reduce problems associated with variations in sample mixing, localized heating, and photodissociation. However, the major drawbacks of using metal colloids for SERS-based assays are their lack of chemical affinity for the target analyte in solution and problems associated with non-specific adsorption that complicate detection.[19-21] The random aggregation of nanoparticles is also known to affect the reproducibility of the acquired SERS spectrum.[17, 22, 23] Under these conditions, SERS measurements are recorded using extended acquisition times greater or equal to one second to improve limits of detection, but limiting throughput.

Two dimensional planar substrates avoid many complications associated with nanoparticles. However, the limit of detection of 2-D substrates in solution is still controlled by transport, which can hinder analyte interaction with the SERS-active surface.[24] Over the years, methods have been developed to increase substrate-analyte interactions. Chemical modifications have been shown to increase affinity of the analyte molecules for the SERS substrate.[17, 23, 25-29] Such techniques concentrate nanoparticle-analyte conjugates in the detection volume to improve detection, but are limited to analytes with high affinity for the functionalized surface. Other techniques actively concentrate nanoparticle-analyte conjugates into the detection volume using electrokinetic or magnetic forces.[25, 30-35] Although these techniques improve sensitivity and the functionality of the SERS assays, the incorporation of active elements or additional fabrication steps add cost and complexity to the final device. Despite the recent advances in performance and sensitivity, these inherent drawbacks limit the successful translation of SERS from the research lab to practical applications.

Hydrodynamic focusing is another technique that can confine analytes near a surface. The interaction of two fluid streams at different velocities will confine the contents of the slow moving fluid into a volume defined by the flow ratio of the two merging streams. The faster moving stream, or sheath flow, is commonly used in commercial flow cytometer instruments to confine cells and particles prior to their passing through the detection volume one at a time.[36] Capillary electrophoresis with laser-induced fluorescence in a sheath-flow cuvette has been shown to effectively confine analyte molecules into the excitation/detection volume, enabling fluorescence detection at femtomolar concentrations.[37, 38] Ligler and colleagues showed that confining a high-conductivity fluid over electrodes improved conductivity measurements in a microchip flow cytometer.[39] Similarly, Manz and coworkers demonstrated the potential of hydrodynamic focusing to provide efficient sample delivery to immunoassays on surfaces.[40] In this study, the confinement of the sample fluid near the surface promotes interaction between the sample molecules and the SERS substrate.

Given the surface sensitivity of SERS, sample confinement with hydrodynamic focusing on planar surfaces may facilitate SERS detection in flow. In this study, the combination of finite element simulations, fluorescence imaging, and Raman experiments are used to investigate the improvement in SERS sensitivity. Our results show rapid and efficient detection of rhodamine 6G (R6G) eluted from a capillary and confined onto a SERS-active substrate located at the bottom of the channel using a faster moving sheath flow around the sample capillary outlet.

EXPERIMENTAL METHODS

Material and Reagents

Rhodamine 6G (R6G, ~95%) was purchased from Sigma-Aldrich (St. Louis, MO). Ultrapure water (18.2 MΩ cm) was obtained from a Barnstead Nanopure filtration system. All other chemicals were of analytical grade and used without any further purification.

Substrate Preparation

SERS-active substrates were fabricated by a previously reported thermal evaporation procedure.[41] These substrates were incorporated into a custom-built flow cell by affixing individual substrates onto a standard microscope slide with two 3 mm diameter holes predrilled 35 mm along the center of the slide. Prior to its use, the SERS substrate on the glass slide was soaked overnight in 0.1 M NaOH (Sigma-Aldrich, 99.99%) to dissolve the anodized aluminum oxide (AAO) filter. The resulting SERS-active substrate was thoroughly rinsed with ethanol (Sigma-Aldrich, 99.5%) followed by a final rinse with ultrapure water.

Flow Cell Assembly and SERS Detector

Figure S1 (see Supporting Information) shows a schematic diagram of the experimental setup. The homebuilt flow cell consists of a FEP plastic base plate, a SERS substrate, and a 250 μm thick silicone gasket with a 2 mm slit cut that defined the flow channel, and a stainless steel top plate. The end of a fused silica capillary (Polymicro Technologies, Phoenix AZ) with 72 μm i.d., 143 μm o.d. , and ~50 cm long was tightly clamped in between the gasket and the substrate to deliver the sample into the detection region. The sample was pressure driven through the capillary at a flow rate of 5 μL/min using a custom-made injection block.[42] Hydrodynamic focusing of the sample stream inside the flow chamber was achieved by pumping the sheath liquid (water) continuously through the flow chamber via the inlet port located on the base plate. The sheath liquid flow rate was controlled using a syringe pump (Model NE-500 OEM, New Era Pump Systems Inc., Farmingdale, NY) controlled by LabView (National Instruments, Austin, TX). The liquid was drained out of the flow chamber via the outlet channel connected to the waste reservoir. The flow channel was sealed with a standard cover glass, pressed by the top plate, and secured using 4 tensioning screws.

Raman Measurements

Raman measurements were performed using a previously described home-built system.[41] The sample was illuminated through a 40X water-immersion objective (Olympus, NA= 0.8), resulting in a spot size of approximately 0.4 μm^2. The power of the 632.8 nm HeNe laser was ~1.2 mW, as measured at the sample. Raman back-scattering signal was collected into the same objective lens and directed to the spectrograph and EMCCD (Newton 970, Andor). The flow cell was positioned on the microscope stage and the sheath flow was enabled using the syringe pump. 4000 spectra were recorded in kinetic series with 50 ms acquisition times.

Fluorescence Imaging

Wide-field fluorescence images were acquired using the same microscope described in the Supporting Information with the following modifications. A 455 nm diode lamp was epi-illuminated onto the sample using a 532 nm laser BrightLine® single-edge laser-flat dichroic beamsplitter (Semrock) and a 10X objective (Olympus, NA=0.5). For this experiment, the capillary was pinned directly to a glass slide in the flow cell. The fluorescent signal was collected through the same objective lens and transmitted back consecutively through the dichroic beamsplitter and a 532 nm RazorEdge® long pass filter (Semrock) before being recorded by an Optixcam summit series 5MP digital camera (Microscope Store, Virginia, USA). Images were recorded at different sheath flow rates using the OC View imaging software.

Data Analysis

Off-line spectral preprocessing and analysis were performed as described in the Supporting Information.

COMSOL Simulations

The fluid dynamics inside the flow chamber was modeled using commercial finite element analysis software, Comsol Multiphysics 4.2a, (COMSOL Inc., Burlington, MA). A cross-sectional 3-D model was designed in the CAD environment, assuming lateral symmetry as modeled by a mirror plane. The CAD geometry described a cylindrical tube inside a rectangular channel with dimensions matching those of the capillary inside the flow channel. Two equations described the model: Navier-Stokes equations at steady state calculated in the Laminar Flow physics interface, and Fick's law for steady state diffusive transport of solute molecules in the capillary and the flow cell calculated in the Transport of Diluted Species physics interface. For the flow equation, the boundary conditions include zero velocity at the wall, constant flow rates at the two inlets, pressure with vanishing viscous stress at the flow cell outlet, and continuity boundary condition at the capillary outlet. For the mass transport, the concentration boundary condition is applied to the capillary inlet (1 mM) and flow cell outlet (0 mM). The symmetry and cell walls were modeled with zero normal flux condition. With solute species in relatively low concentrations compared to the solvent (water), it is assumed that a change in solute concentration does not influence the fluids's density and viscosity. This implies that it is possible to solve first for the fluid flow and then for the mass transport. In this model, the solution to the flow equation was used to solve the mass transport equation.

RESULTS AND DISCUSSION

Modeling and Fluorescence Images of Hydrodynamic Focusing on a Surface

The confinement effects demonstrated with hydrodynamic focusing to improve measurement sensitivity in microfluidics-based assays suggest the potential of using this method to improve SERS detection in flow. Finite element simulations were combined with wide-field fluorescence imaging experiments to assess the influence of hydrodynamic focusing on fluid dynamics near the SERS surface.

COMSOL simulations were performed to model the effect of sheath liquid flow dynamics on the sample stream eluting from a capillary placed laterally on a surface. In these calculations, the ratio of the sheath flow rate to that of the sample analyte was varied to assess the analyte confinement onto the surface, where SERS detection occurs. Figure 1 presents juxtaposed images from the COMSOL simulation in the xy-plane (left) and the corresponding wide-field fluorescence images (right) acquired under equivalent conditions. The first row in Figure 1 depicts a schematic representation of the analyte eluting from the

sample capillary under the influence of the surrounding sheath flow in a COMSOL simulation (Figure 1a) and a wide-field fluorescence image (Figure 1b). The experiment was modeled at varying sheath flow rates while the capillary flow was held at a constant rate. Wide-field fluorescence of R6G eluting from the capillary was imaged while varying the sheath flow rate to match the sheath flow rate to capillary flow rate ratios used in the COMSOL simulations. The relative volumetric velocities of the two fluid streams are the important parameter to determine the effect of confinement of the analyte eluted from the capillary by the sheath fluid. [43] The sheath flow to analyte flow rate ratios are 36:1 (Figures 1c and 1d), 10:1 (Figures 1e and 1f), and ~0 (Figures 1g and 1h), respectively.

Using a flow rate ratio of 36:1, the COMSOL simulation predicts a narrow profile for the sample eluting out of the sample capillary (Figure 1c). The fluorescence image acquired under equivalent conditions (Figure 1d) shows that the R6G molecules dispensed by the capillary are confined into a cone-like profile by the interaction with the faster moving sheath flow, as predicted. A sheath flow to capillary flow rate ratio of 10:1 results in a broader longitudinal stream of analyte molecules with a width similar to the capillary outer diameter that also matches the model. When the capillary flow rate is greater than sheath fluid velocity, the sample expands and essentially fills the flow chamber. This behavior is clearly observed in both the COMSOL simulation (Figure 1g) and in the wide field fluorescence images (Figure 1h).

The fluid dynamics simulations provide insight in the confinement of the sample normal to the surface. Figure 2 shows a schematic representation of the flow cell and its components in the xz-plane, normal to the SERS substrate (Figure 2a) as well as the simulation results for sheath flow rate to capillary flow rate ratios of 10:1 (Figure 2b), 36:1 (Figure 2c), and 72:1 (Figure 2d), respectively. The initial increase in the sheath flow shows the expected increase in sample confinement in the z-direction. The sample stream thickness can be calculated from classical hydrodynamics and is related to the ratio of the sheath flow and sample flow rates. With confinement on the surface, the slowed velocity at the walls results in a thicker sample layer. Manz and coworkers accounted for the wall velocity and demonstrated the ratio between the total (Q_{total}) and sample (Q_{sample}) flow rates scales in relation to the sample layer thickness (d) and the height of the channel (h) as follows[44]:

$$\frac{Q_{sample}}{Q_{Total}} = 3\frac{d^2}{h^2} - 2\frac{d^3}{h^3} \quad (1)$$

The layer thickness as a function of sheath flow rate can be determined by solving Eq. 1 for d, using a fixed sample flow rate (5 μL/min) and a channel height of 250 μm (see Figure S2 in Supporting Information). Under these conditions, the faster sheath flow confines the molecules into a narrower stream of analyte molecules over the surface.

The simulation of our experimental geometry shows that an optimum sheath flow rate is observed at a ratio of 36:1. Figure 2d shows the COMSOL simulation at a flow rate ratio of 72:1. At this faster sheath flow rate, there is increased focusing in the xy-plane parallel to the surface; however, the simulation shows decreased analyte concentration on the SERS substrate from what appears to be turbulent flow (Figure 2d). The sharp edges of the capillary in the flow channel appear to induce turbulence when the sheath flow rate to sample flow rate ratio exceeds 36:1. In the given cell configuration, the onset of turbulence appears to limit the extent of sample confinement associated with hydrodynamic focusing.

The agreement between the fluorescence images and finite-element models show that sample confinement is achieved by hydrodynamic focusing in our SERS flow detector. The COMSOL model indicates the analyte concentration is conserved over finite dimensions as

it exits the capillary. From the COMSOL simulation, it is evident that SERS collection should be performed at a distance within 100-200 μm, approximately equal to the sample capillary o.d., which is easily identified in the microscope. The combination of COMSOL simulations and wide-field fluorescence imaging experiments suggests that confinement of molecules at the bottom of the flow channel could improve SERS detection under controlled conditions.

Improved SERS Detection Using Hydrodynamic Focusing

A series of Raman experiments were performed to assess the sensitivity of the SERS flow detector. R6G was used as the standard model molecule due to its large Raman cross section.[7, 8, 45, 46]

To determine the influence of the sheath flow on the SERS signal, the intensity of a 10^{-5} M R6G solution eluted from the capillary was measured at different sheath flow rates. Figure 3 shows a plot of the absolute area of the bands at 1175, 1306, 1357, 1506, and 1648 cm^{-1} in the SERS spectrum of R6G (shown in Figure 4) as a function of sheath flow rate. The bands in the SERS spectrum of R6G used to quantify the SERS intensity are associated with the characteristic stretching modes of C-H band, C=N, and aromatic C-C stretching bands of R6G, respectively.[5, 45, 47-49]

The plot shown in Figure 3 reveals two distinct behaviors. The first portion of the plot demonstrates that increasing the sheath flow rate from 0 to 180 μL/min results in a nonlinear increase in integrated SERS intensity for all five bands in the spectrum of R6G. The sample elutes from the capillary at 5 μL/min, providing a sheath to analyte flow rate ratio of 36:1. This observation is in agreement with the prediction that increasing the sheath flow promotes confinement of analyte molecules eluted from the capillary onto the SERS substrate. As confinement increases, a significant increase in SERS intensity is observed.

As the sheath flow rate is increased further, a marked drop in SERS intensity is noted. The drop in SERS intensity may arise from different effects. First, faster sheath flow decreases the dwell time of the analyte in the SERS-active region, hence limiting signal throughput in the detection volume. Second, the COMSOL simulation suggests turbulent flow at higher sheath flow rates, which may also disturb the concentration of analyte molecules at the SERS-active substrate. Under these conditions, molecules are swept into the sheath fluid before reaching the bottom of the channel where the SERS signal is generated. The results in Figure 3 agree with the COMSOL simulations and indicate optimal conditions for SERS detection.

The increase in signal associated with the sheath flow detector is different than what is predicted for convective-diffusive, or advective, transport to a surface. Matsuda solved the advective transport to a surface for a thin layer cell as follows[50, 51]:

$$J = 1.47\left(\frac{DA}{h}\right)^{2/3} CQ^{1/3} \quad (2)$$

where D is the diffusion coefficient, A is the area of the surface used for detection, h is the height of the channel, C is the sample concentration, and Q is the volumetric flow rate. Increased flow rate should show nonlinear increase reaching a limit, as is observed in our flow cell when the analyte is introduced through the main flow channel (see Figure S3 in Supporting Information). The increase in signal observed in the sheath-flow detector shows behavior that resembles increased interactions at the walls associated with confined geometries. In confined channels, adsorption efficiency is reported to increase proportional to the cross-sectional area of the channel.[50] Decreased cross-sectional area improves the

efficiency of molecules diffusing to the surface. This behavior suggests that increased transport to the SERS surface plays a role in our detector, which we will investigate further below.

Flow Cell Sensitivity and Limit of Detection

Our results suggest that hydrodynamic focusing gives rise to the greatest SERS signal at a sheath flow rate of 180 μL/min. Figure 4a shows a 50 ms SERS spectrum of a 10^{-5} M R6G solution acquired under the optimized conditions. The main features of the R6G spectrum are the bands at 1175, 1306, 1357, 1506, and 1648 cm^{-1} highlighted with the dashed vertical lines. The number and position of the bands in the SERS spectra shown in Figure 4a are in agreement with those reported from SERS studies of R6G.[5, 45, 47-49] Using our SERS detector, we have successfully detected R6G in a 1 nM solution. Figure 4b shows an average of ten 50 ms spectrum of a 10^{-9} M R6G solution acquired under the same conditions. The 10^{-9} M R6G averaged spectrum shows a relatively high noise, suggesting this concentration is near the limit of detection. However, the Raman bands of R6G can be distinguished from the background spectrum shown in Figure 4c, demonstrating the high level of sensitivity of the assay at nanomolar concentrations using a short (50 ms) spectral acquisition time.

To assess the improvement in SERS detection using hydrodynamic focusing, the SERS intensity of R6G was measured by injecting the dye analyte into the flow cell without the capillary. For this control experiment, the injection flow rate was optimized to give the highest SERS signal (see Figure S3 in Supporting Information). It was found that in the absence of sheath flow confinement, injecting a 10^{-5} M R6G solution at a flow rate of 150 μL/min gave rise to the greatest SERS intensity. Figure 4d shows a 50 ms SERS spectrum of a 10^{-5} M R6G solution acquired under these conditions. The interpretation of this spectrum follows directly from the discussion of the 10^{-5} M R6G spectrum shown in Figure 4a. The two R6G spectra show similar SERS intensity at 10^{-5} M. However, the detection limit of the R6G SERS signal is greatly reduced when the sample is introduced directly into the flow cell by syringe pump injection. Figure 4e shows an average of ten 50 ms spectrum of a 10^{-6} M R6G solution. As evident, the R6G SERS signal at this concentration is above the background (Figure 4f) but near the limit of detection. The results from Figure 4 demonstrate that the use of hydrodynamic focusing improves the limit of detection by three orders of magnitude compared to simply flowing the analyte over the SERS surface in a larger channel. The limit of detection with hydrodynamic focusing is also three orders of magnitude better than previous reports of R6G with 2-D planar SERS substrates in flow.[12]

In addition to providing a lower limit of detection, the use of a narrow-bore capillary for sample delivery greatly reduces the required sample volume by four orders of magnitude: ~100 nL instead of ~1 mL when injecting the sample in the flow cell.

The sensitivity of the detector was further investigated by measuring the SERS spectrum of R6G solutions ranging from 1×10^{-4} to 1×10^{-9} M. Figure 5 shows the log-log plot of the integrated SERS intensity as a function of R6G concentration at each Raman shift frequency. As expected, the plot reveals an increase in band area for all five Raman bands at increasing R6G concentration. Interestingly, the plot does not follow the Langmuir adsorption isotherm typically observed for SERS experiments. Instead, two different sensitivity regimes can be distinguished for each of the 5 bands. The first regime displays a linear increase in integrated SERS intensity of R6G at low concentration (10^{-9} to 10^{-6} M). The inset in Figure 5 (plotted in linear scale) demonstrates the linear dependence of the SERS signal as a function of R6G concentration. The averaged Raman band areas at 1175, 1306, 1357, 1506, and 1648 cm^{-1} over this concentration range have R^2 values of 0.9580, 0.9808, 0.9678, 0.9736, and 0.9608, respectively. These regression coefficients support the

linearity of the data and demonstrate that the SERS-based flow detector can quantitatively detect R6G in a linear fashion for concentrations ranging from 10^{-6} to 10^{-9} M.

The second regime appears to show an exponential increase in SERS signal for concentrations greater than 10^{-6} M. At these higher concentrations, adsorption to the surface is prominently observed, suggesting more complete monolayer or potentially multilayer effects. Chemical interactions between the R6G molecules and the metallic surface may give rise to additional chemical enhancements that produce the steep increase in signal for concentrations higher than 10^{-6} M; however, the relative band intensities and frequencies are unchanged at these higher concentrations arguing against a new complex formation at higher concentrations.

Flow Cell Regeneration

The results presented above suggest that adsorption to the surface plays a role in the increased sensitivity. For high throughput analysis, it is desirable to desorb molecules after detection. One of the advantages of the flow detector is the analyte stream is rapidly depleted of molecules when the sample stream is changed. This attribute of flow detection prevents pooling of analyte molecules. To test the adsorption and desorption properties of the detector, the area of the five Raman bands in the spectrum of R6G was monitored during the course of an experiment where R6G was pumped in, the analyte flow was stopped, and then the cell was flushed with 0.1 M NaOH.

Figure 6A shows the heatmap of the SERS intensity as a function of Raman shift and time for the injection of 10^{-5} M R6G solution, followed by stopping the analyte flow and flushing the sample capillary with NaOH. In Figure 6A, the temporal behavior of the prominent Raman bands can be divided into five time segments. The first segment corresponds to the first 45 seconds of spectral acquisition and represents the time needed for the 10^{-5} M R6G solution in the injection block to travel through the capillary and reach the detection volume in the flow channel (1). The presence of R6G in the detection volume results in an increase in SERS signal followed by an intensity plateau for all five bands from t=45 to 100 sec, as seen in the second segment (2). At t=100 sec, the injection of R6G is stopped, resulting in a rapid decrease in signal for all the bands, as seen in the third segment (3). During this decrease in SERS signal, the analyte in the injection block was changed to a 0.1 M solution of NaOH. At t=150 sec, NaOH was injected into the capillary to flush out the residual R6G present in the capillary, resulting in a second increase in SERS signal from t=150 to 200 sec (4). The last segment (5) corresponds to the elution of NaOH into the detection volume, which results in a rapid decrease in integrated SERS intensity and the return of the signal to baseline level.

Figure 6B shows the SERS intensity profile at 1357 cm^{-1} (black trace) as a function of acquisition time extracted from Figure 6A. Analysis of the 1357 cm^{-1} intensity enables quantification of adsorption and desorption rates in the experiment. To determine the on (Δt_m) and off (Δt_{-m}) times at which adsorption and desorption of R6G take place, a 9-point Savitzky-Golay filter was applied minimize noise, as indicate by the red trace (Figure 6B). Δt equals the time needed for the R6G SERS signal to change between 10% and 90% of its maximum signal intensity. The on times resulting from the increase in R6G signal following the first (Δt_m) and second ($\Delta t_{m'}$) injection extracted from the red trace were determined to be 8 and 7 seconds, respectively. The on-rate is observed reproducibly as expected. Conversely, the off times resulting from the first decrease in R6G signal (Δt_{-m}) when the first injection was stopped and the second increase in R6G signal ($\Delta t_{-m'}$) following NaOH injection were determined to be 15 and 6 seconds, respectively. Interestingly, the $\Delta t_{-m'}$ was found to be much less than Δt_{-m}, suggesting different desorption mechanisms. Injecting NaOH through the capillary likely displaces the R6G, promoting faster desorption and return of the SERS

signal to baseline level. The mechanism of desorption in the absence of NaOH is less clear. There is the possibility that the molecules are photo-degraded, though no evidence of carbonaceous contamination is observed. Any photo-degraded molecules could be swept away by the flow before they can be detected. A second possibility is local heating of the plasmonic surface promotes dissociation. We are still investigating the origins of the desorption mechanism.

The results from Figure 6 demonstrate at least two mechanisms for regenerating the SERS surface for subsequent detection. The baseline signals in segments 3 and 5 in Figures 6A and 6B show evidence that the R6G molecules are completely desorbed from the silver substrate.

Origin of Increased Sensitivity

The origin of the increased sensitivity at low R6G concentrations appears to arise from improved mass transport and adsorption of analyte to the surface. As noted in the introduction, hydrodynamic focusing confines analyte molecules into a region near the sensor surface, resulting in increased interactions with the intense electric field at the surface. The COMSOL model shows the confinement effect; however, the model does not account for analyte absorption, to which we attribute the increased sensitivity. It has been previously reported that mass transport to the surface is optimized when the sample layer matches distances associated with diffusion.[40] The nonlinear increase in signal observed with increased confinement (faster sheath flow) supports the idea that increased adsorption efficiency occurs. Adsorption efficiency is aided by constant renewal of the analyte flowing over the surface. As molecules adsorb, the local concentration at the surface increases. Faster adsorption (transport to the surface) results in more molecules in the detection volume and increased signals.

In the absence of adsorption, there should be no advantage to sample confinement. Since most molecules adsorb to silver, the increased signals should transfer to other samples in a straightforward manner.

CONCLUSION

A simple and effective approach for rapid, high throughput SERS detection has been demonstrated using hydrodynamic focusing. The use of sheath flow over a capillary on a surface confines analyte molecules eluted from the capillary over a SERS substrate on the bottom of the flow cell, resulting in greatly improved detection. Simulations and wide-field fluorescence imaging were used in combination to confirm the confinement and determine optimum parameters for SERS detection. Using a 2-D planar substrate, high throughput flow detection of R6G was demonstrated at nanomolar concentrations with acquisition times as short as 50 ms. The current SERS detection strategy provides advantages over the use of colloidal mixtures as sequential on and off detection of R6G was achieved without significant “memory effect” or fouling of the SERS substrate. Additionally, the volume of sample needed for analysis using our flow detector is significantly reduced.

The ultrasensitive on-line SERS detector presented here will be straightforward to implement with measurements in flow, such as chromatographic separations. Given the robustness, sample requirement, simplicity, sensitivity, and reproducibility of the current SERS detector, future work will assess the applicability of this SERS detection platform to diverse problems in chemical analysis.

Supplementary Material

Refer to Web version on PubMed Central for supplementary material.

Acknowledgments

The University of Notre Dame and the NIH Award R21 GM107893 supported the work. The authors thank the referees for helping improve this manuscript through the review process.

REFERENCES

1. Kneipp K, Kneipp H, I. I, Dasari RR, Feld MS. Chem Rev. 1999; 99:2957–+. [PubMed: 11749507]
2. Moskovits M. Reviews of Modern Physics. 1985; 57:783–826.
3. Stiles PL, Dieringer JA, Shah NC, Van Duyne RR. Annu Rev Anal Chem. 2008; 1:601–626.
4. Dieringer JAW, K. L. Masiello DJ, Camden JP, Kleinman SL, Schatz GC, Van Duyne RP. J. Am. Chem. Soc. 2008; 131:849–854. [PubMed: 19140802]
5. Kneipp K, Wang Y, Kneipp H, Perelman LT, Itzkan I, Dasari R, Feld MS. Phys. Rev. Lett. 1997; 78:1667–1670.
6. McGuinness CD, Macmillan AM, Karolin J, Smith WE, Graham D, Pickup JC, Birch DJS. Analyst. 2007; 132:633–634. [PubMed: 17592580]
7. Michaels AM, Nirmal M, Brus LE. J Am Chem Soc. 1999; 121:9932–9939.
8. Nie SM, Emery SR. Science. 1997; 275:1102–1106. [PubMed: 9027306]
9. Dieringer JA, McFarland AD, Shah NC, Stuart DA, Whitney AV, Yonzon CR, Young MA, Zhang XY, Van Duyne RP. Faraday Discuss. 2006; 132:9–26. [PubMed: 16833104]
10. Lal S, Grady NK, Goodrich GP, Halas NJ. Nano Lett. 2006; 6:2338–2343. [PubMed: 17034107]
11. McFarland AD, Young MA, Dieringer JA, Van Duyne RP. J. Phys. Chem. B. 2005; 109:11279–11285. [PubMed: 16852377]
12. Leopold N, Lendl B. Anal. Bioanal. Chem. 2010; 396:2341–2348. [PubMed: 20127318]
13. Lee S, Choi J, Chen L, Park B, Kyong JB, Seong GH, Choo J, Lee Y, Shin KH, Lee EK, Joo SW, Lee KH. Anal Chim Acta. 2007; 590:139–144. [PubMed: 17448337]
14. Park T, Lee S, Seong GH, Choo J, Lee EK, Kim YS, Ji WH, Hwang SY, Gweon DG, Lee S. Lab Chip. 2005; 5:437–442. [PubMed: 15791342]
15. Strehle KR, Cialla D, Rösch P, Henkel T, Köhler M, Popp J. Anal. Chem. 2007; 79:1542–1547. [PubMed: 17297953]
16. Wang M, Benford M, Jing N, Cote G, Kameoka J. Microfluid Nanofluid. 2009; 6:411–417.
17. Wang M, Jing N, Chou IH, Cote GL, Kameoka J. Lab Chip. 2007; 7:630–2. [PubMed: 17476383]
18. Wilson R, Monaghan P, Bowden SA, Parnell J, Cooper JM. Anal Chem. 2007; 79:7036–7041. [PubMed: 17711297]
19. Measor P, Seballos L, Yin DL, Zhang JZ, Lunt EJ, Hawkins AR, Schmidt H. Appl Phys Lett. 2007; 90
20. Oo MKK, Han Y, Kanka J, Sukhishvili S, Du H. Opt Lett. 2010; 35:466–468. [PubMed: 20160786]
21. Yang X, Shi C, Wheeler D, Newhouse R, Chen B, Zhang JZ, Gu C. J Opt Soc Am A. 2010; 27:977–984.
22. Bell SE, Sirimuthu NM. Chemical Society reviews. 2008; 37:1012–24. [PubMed: 18443686]
23. Liu JK, White I, DeVoe DL. Anal Chem. 2011; 83:2119–2124. [PubMed: 21322579]
24. Asiala SM, Schultz ZD. Chem Commun (Camb). 2013; 49:4340–2. [PubMed: 23103901]
25. Choi I, Huh YS, Erickson D. Lab Chip. 2011; 11:632–638. [PubMed: 21120240]
26. Chou IH, Benford M, Beier HT, Cote GL, Wang M, Jing N, Kameoka J, Good TA. Nano Lett. 2008; 8:1729–1735. [PubMed: 18489171]
27. Guo YB, Oo MKK, Reddy K, Fan XD. Acs Nano. 2012; 6:381–388. [PubMed: 22176766]
28. Park SM, Huh YS, Craighead HG, Erickson D. P Natl Acad Sci USA. 2009; 106:15549–15554.

29. Yazdi SH, White IM. Anal Chem. 2012; 84:7992–7998. [PubMed: 22924879]
30. Cho HS, Lee B, Liu GL, Agarwal A, Lee LP. Lab Chip. 2009; 9:3360–3363. [PubMed: 19904401]
31. Chrimes AF, Kayani AA, Khoshmanesh K, Stoddart PR, Mulvaney P, Mitchell A, Kalantar-zadeh K. Lab Chip. 2011; 11:921–928. [PubMed: 21267497]
32. Han B, Choi N, Kim KH, Lim DW, Choo J. J Phys Chem C. 2011; 115:6290–6296.
33. Huh YS, Chung AJ, Cordovez B, Erickson D. Lab Chip. 2009; 9:433–439. [PubMed: 19156293]
34. Hwang H, Han D, Oh YJ, Cho YK, Jeong KH, Park JK. Lab Chip. 2011; 11:2518–2525. [PubMed: 21674105]
35. Lowe AJ, Huh YS, Strickland AD, Erickson D, Batt CA. Anal Chem. 2010; 82:5810–5814. [PubMed: 20527817]
36. Shapiro, HM. Practical Flow Cytometry. 4th ed.. John Wiley & Sons; Hoboken, New Jersey: 2003.
37. Cheng YF, Dovichi NJ. Science. 1988; 242:562–4. [PubMed: 3140381]
38. Dada OO, Huge BJ, Dovichi NJ. Analyst. 2012; 137:3099–3101. [PubMed: 22606689]
39. Golden JP, Justin GA, Nasir M, Ligler FS. Anal Bioanal Chem. 2012; 402:325–335. [PubMed: 21952728]
40. Hofmann O, Voirin G, Niedermann P, Manz A. Anal Chem. 2002; 74:5243–5250. [PubMed: 12403577]
41. Asiala SM, Schultz ZD. Analyst. 2011; 136:4472–4479. [PubMed: 21946698]
42. Krylov SN, Starke DA, Arriaga EA, Zhang Z, Chan NW, Palcic MM, Dovichi NJ. Anal Chem. 2000; 72:872–877. [PubMed: 10701276]
43. Chang CC, Huang ZX, Yang RJ. J Micromech Microeng. 2007; 17:1479–1486.
44. Hofmann O, Niedermann P, Manz A. Lab Chip. 2001; 1:108–114. [PubMed: 15100869]
45. Hildebrandt P, Stockburger M. J Phys Chem-Us. 1984; 88:5935–5944.
46. Kneipp K, Wang Y, Dasari RR, Feld MS. Appl Spectrosc. 1995; 49:780–784.
47. Liu GL, Lee LP. Appl Phys Lett. 2005; 87
48. Pristinski D, Tan SL, Erol M, Du H, Sukhishvili S. J Raman Spectrosc. 2006; 37:762–770.
49. Tao A, Kim F, Hess C, Goldberger J, He RR, Sun YG, Xia YN, Yang PD. Nano Lett. 2003; 3:1229–1233.
50. Sjolander S, Urbaniczky C. Anal. Chem. 1991; 63:2338–2345. [PubMed: 1759716]
51. Matsuda H. Journal of Electroanalytical Chemistry. 1967; 15:325–336.

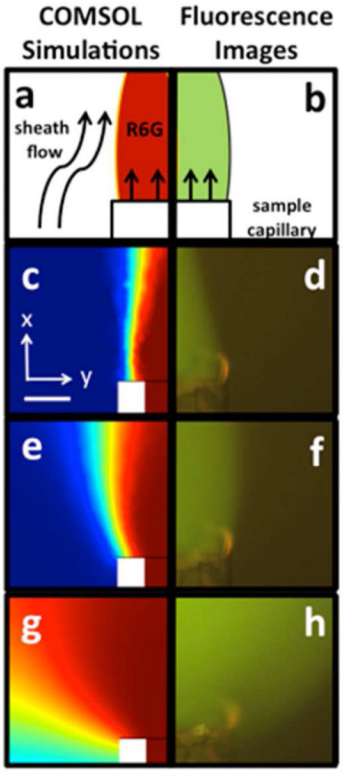

Figure 1.

Schematic representation of a COMSOL simulation (a) and a wide-field fluorescence image (b) showing the analyte eluting from the sample capillary under the influence of the surrounding sheath flow. COMSOL simulations (left panels) showing analyte concentration with corresponding wide-field fluorescence images (right panels) in the xy-plane are depicted at sheath flow rate to capillary flow rate ratios of 36:1 (c) and (d), 10:1 (e) and (f), and ~0 (g) and (h), respectively. The capillary flow rate was held constant. The dimensions and parameter ratios were kept identical for the fluorescence experiments and the COMSOL simulations. The concentration intensity scales from zero concentration (blue) to 1 mM concentration (red) in the COMSOL simulations. Scale bar = 75 micrometers.

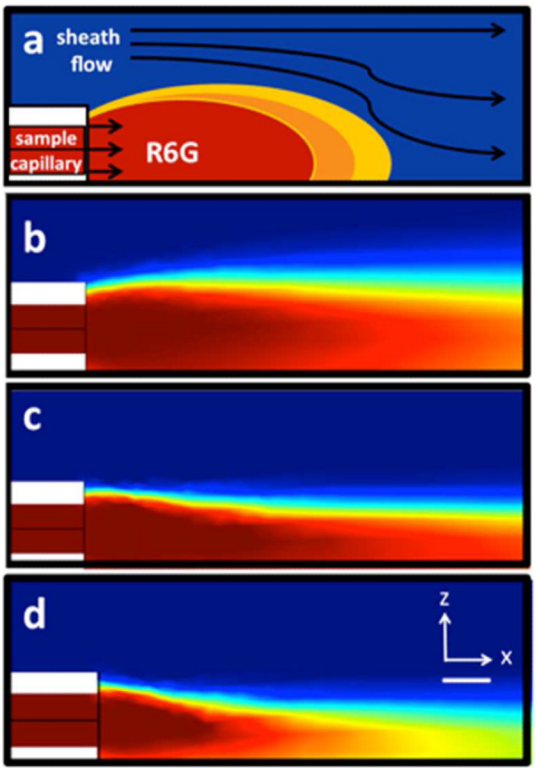

Figure 2.
(a) The flow cell and its components in the xz-plane, normal to the SERS substrate, are shown schematically. COMSOL simulations show the confinement and the predicted analyte concentration at different sheath flow to capillary flow rates. The sheath flow rate to capillary flow rate ratios depicted are: (b) 10:1, (c) 36:1, and (d) 72:1, respectively. The capillary flow rate was held constant. The concentration intensity scales from zero concentration (blue) to 1 mM concentration (red). Scale bar = 75 micrometers.

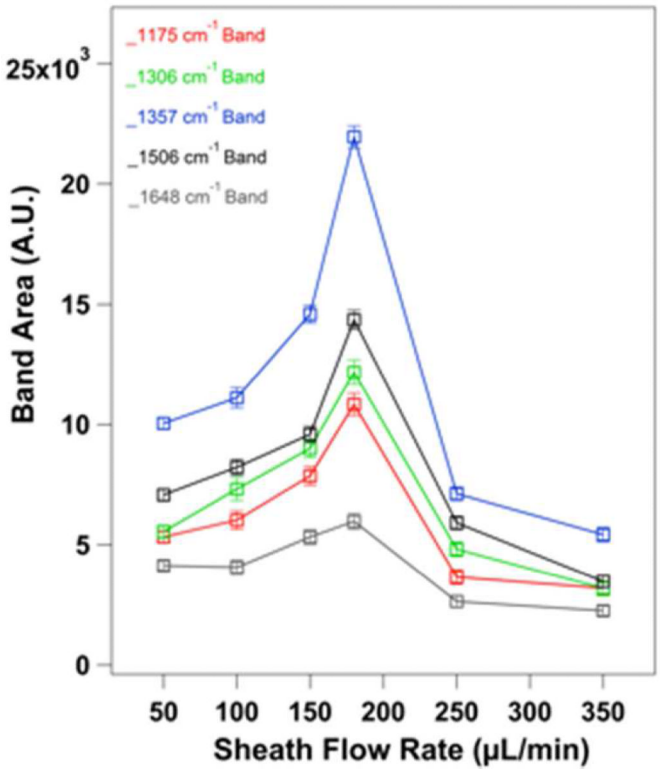

Figure 3.

The areas of the Raman bands at 1174, 1306, 1357, 1506, and 1648 cm^{-1} observed in the SERS spectrum of R6G are plotted as a function of sheath flow rate in the range from 0 to 360 µL/min. The capillary flow rate was held constant at 5 µL/min. Each data point represents the average area of a band taken from 1500 spectra consecutively acquired at 50 ms intervals. Error bars represent the standard deviation.

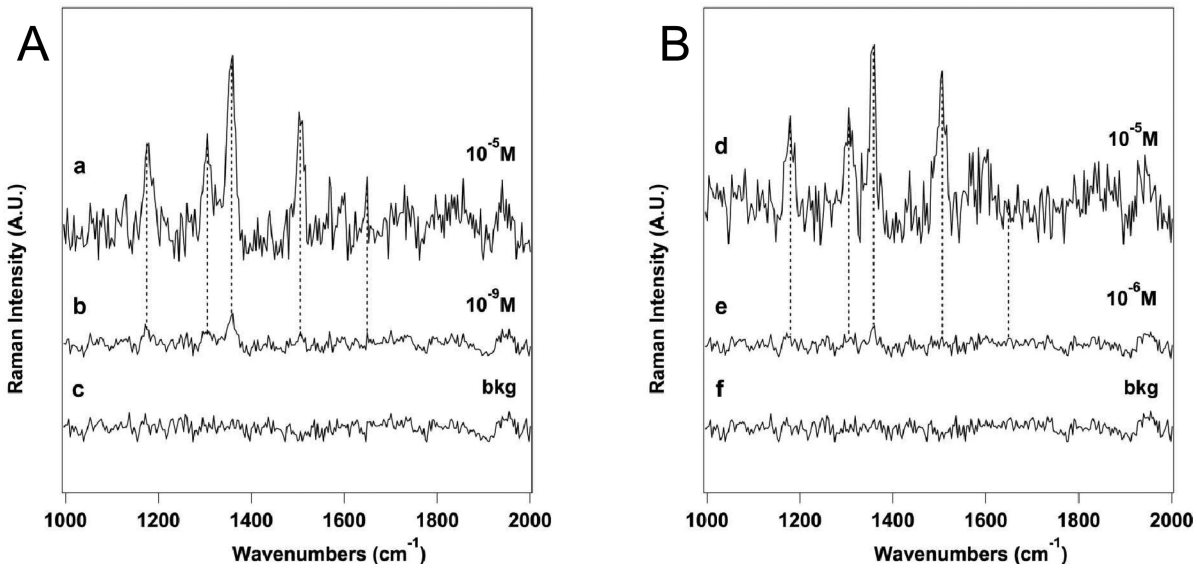

Figure 4.

Spectra obtained with (A) and without (B) hydrodynamic focusing show the increased detection limit achieved with sample confinement. (a) Single SERS spectrum of a 10^{-5} M R6G solution, (b) average SERS spectrum of a 10^{-9} M R6G solution, and (c) background SERS spectrum collected using a 50 ms spectral acquisition and a sheath flow rate of 180 μL/min. (d) Single SERS spectrum of a 10^{-5} M R6G solution, (e) average SERS spectrum of a 10^{-6} M R6G solution, and (c) background SERS spectrum collected using a 50 ms spectral acquisition and by flowing the analyte in the flow cell at a flow rate of 150 μL/min. SERS spectra shown in (b) and (e) are averages of 10 individual, 50 ms SERS spectra. The dashed vertical lines in denote the five R6G bands used for analysis.

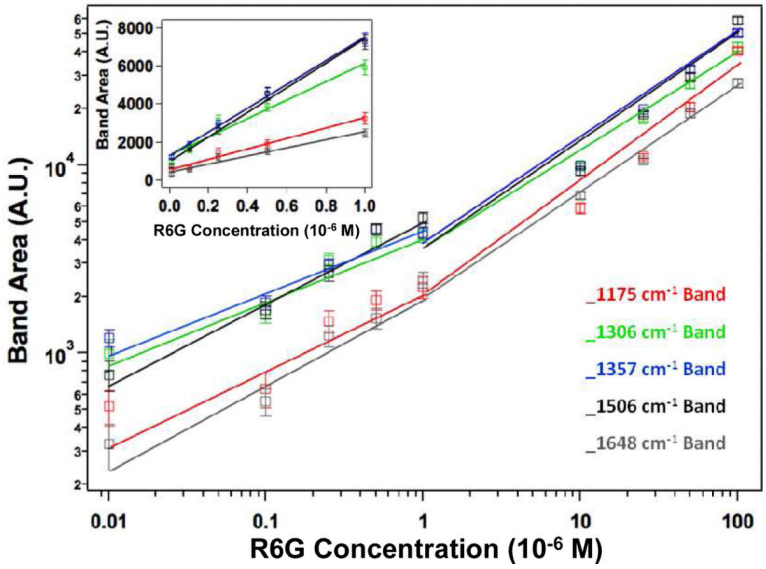

Figure 5.

Log-log plot of the integrated SERS intensity as a function of R6G concentration in the range from 10^{-4} to 10^{-9} M at each Raman shift frequency. The lines are the fit to an exponential for the two different intensity profile. The inset (plotted in linear scale) shows a linear concentration dependence in integrated SERS intensity for R6G concentrations between 10^{-9} and 10^{-6} M. Each data point represents the average area of a band taken from 1500 spectra consecutively acquired using a 50 ms acquisition and a sheath flow rate of 180 μL/min. Error bars represent the standard deviation.

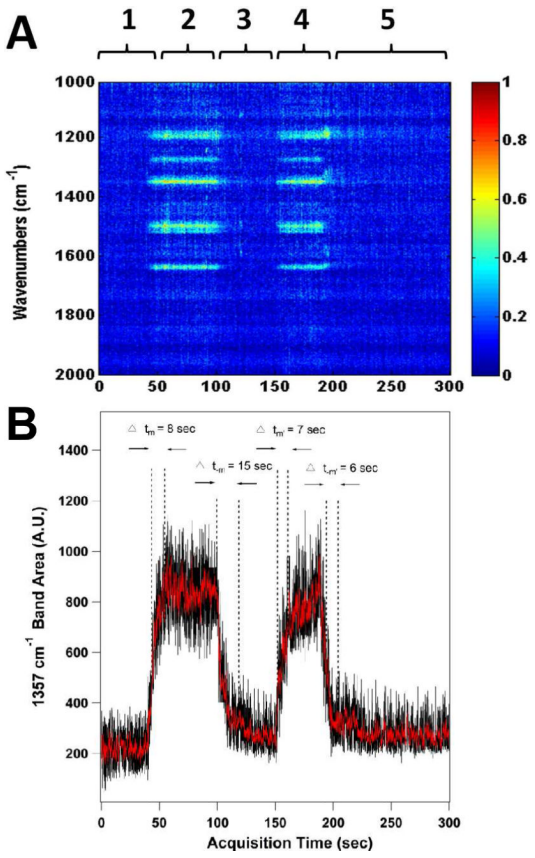

Figure 6.

(A) The heatmap shows the observed SERS intensity at each Raman shift as a function of acquisition time for a 10^{-5} M R6G solution during an experiment where the analyte (1) travels through the capillary, (2) is eluted onto the SERS substrate, (3) analyte flow is stopped and a 0.1M NaOH solution is exchanged for the sample, (4) residual analyte in the capillary elutes, and (5) the NaOH solution is eluted. (B) The SERS intensity profile of a single Raman band (1357 cm^{-1}) as a function of acquisition time is shown, along with the on (Δt_m) and off (Δt_{-m}) times at which adsorption and desorption of R6G take place during the course of the experiment. Of note, the length of segments 1 and 4 are similar, illustrating the time to displace the capillary volume. Spectra were recorded using a 50 ms acquisition and a sheath flow rate of 180 μL/min.